Elastic Shape-from-Template with Spatially Sparse Deforming Forces

Abed Malti[1]   Cédric Herzet[2]

[1] AutoMed/LAT, Université de Tlemcen, Tlemcen, Algeria

[2] INRIA-Rennes, Campus de Beaulieu, Rennes, France

Abstract

Current Elastic SfT (Shape from Template) methods are based on ℓ_2-norm minimization. None can accurately recover the spatial location of the acting forces since ℓ_2-norm based minimization tends to find the best tradeoff among noisy data to fit an elastic model. In this work, we study shapes that are deformed with spatially sparse set of forces. We propose two formulations for a new class of SfT problems dubbed here SLE-SfT (Sparse Linear Elastic-SfT). The First ideal formulation uses an ℓ_0-norm to minimize the cardinal of non-zero components of the deforming forces. The second relaxed formulation uses an ℓ_1-norm to minimize the sum of absolute values of force components. These new formulations do not use Solid Boundary Constraints (SBC) which are usually needed to rigidly position the shape in the frame of the deformed image. We introduce the Projective Elastic Space Property (PESP) that jointly encodes the reprojection constraint and the elastic model. We prove that filling this property is necessary and sufficient for the relaxed formulation to: (i) retrieve the ground-truth 3D deformed shape, (ii) recover the right spatial domain of non-zero deforming forces. (iii) It also proves that we can rigidly place the deformed shape in the image frame without using SBC. Finally, we prove that when filling PESP, resolving the relaxed formulation provides the same ground-truth solution as the ideal formulation. Results with simulated and real data show substantial improvements in recovering the deformed shapes as well as the spatial location of the deforming forces.

1. Introduction

SfT(Shape from Template) is one of the most critical open problems in computer vision of the last decade. The problem is quite challenging since with few adequate priors one must retrieve a 3D deformed shape from a single image. Usually these priors concern the Reprojection Boundary Constraint (*RBC*) and the model of deformation. The former establishes a correspondence between the template shape (known 3D shape) and a deformed image (2D projection of the deformed shape). *RBC* gives the subspace of possible deformed shapes that explains the current deformed image. The latter constrains the possible deforma-

tions of the template given the *RBC*. It allows us to keep one or at most a finite set of plausible deformed shapes [4]. The model prior can differ from physics based to statistics based.

Statistics based approaches usually represent the deformation as a linear combination of learnt shape or mode basis [23, 27, 25, 29, 1]. Physics based approaches were mainly instanciated for isometry [7, 25, 28, 9], conformal [19, 4] and elasticity [14, 21, 2]. It has been theoretically proven that in the case of isometric prior there is a unique solution and in the case of conformal prior there is a set of discrete number of solutions [4]. In the case of elasticity, usually it requires a set of *SBC* (Solid Boundary Constraints). This requirement is necessary to rigidly position the shape in the frame of the deformed image such that we seek only the non-rigid deformation. This constraint ensures that the SfT problem has a unique solution with an ℓ_2-norm linear formulation [20]. It was experimentally shown that a sequential approach does not require *SBC* [2].

Among existing SfT methods, sparsity has already been exploited as a modal prior in the statistics based approaches. It was used to express the deformed shape as a sparse linear combination of the basis shapes. This approach has shown substantial improvement of the reconstruction accuracy [34, 12, 26]. Nevertheless, in this case there is no formal proof that the linear combination is indeed sparse. In physics based SfT and to the best of our knowledge, sparsity has never been used as a spatial prior to characterize such type of deformation. Addressing this class of deformation is important for practical as well as theoretical reasons. In practical terms there is a non-negligible number of daily life deformed objects that might be subjected to sparse deforming forces. For instance clothes, plastic bottles, balloons, etc. In theoretical terms, since the usage of sparsity is here physically justified, it becomes important to formalize it, to investigate the well posedness of it and to provide tools to solve it.

In this paper, we study the formalization and well posedeness of elastic SfT with sparse deforming forces. It is the first time where sparsity is used as a prior to characterize a specific type of spatial deformation. We use a linear elastic model as a physics based prior and a linear formulation with finite element method as suggested in [20]. This previous formulation minimizes the ℓ_2-norm of the force which is applied to obtain the deformed shape. In the case

of sparse deforming force vectors, only few components of these vectors are non-zeros. Thus, such formulation is not appropriate since an ℓ_2-norm minimization may recover a dense deforming force especially in the case of noisy data and errors in modelling. This work provides also a theoretical condition for which the *SBC* is not required to uniquely retrieve the ground-truth 3D deformed shape.

Contributions. We propose two formulations for a new class of SfT problems dubbed here SLE-SfT (Sparse Linear Elastic-SfT). Equation (IF) establishes the Ideal Formulation with the ℓ_0-norm which minimizes the number of non-zeros components of the applied force vector. Equation (RF) states the Relaxed Formulation with an ℓ_1-norm since the ℓ_0-norm is NP-hard to solve [13]. These new formulations do not use *SBC*. We introduce the Projective Elastic Space Property (PESP) that jointly encodes the *RBC* and the elastic model (Definition 2). In Theorem 2, we prove that filling this property is necessary and sufficient for the relaxed formulation to: *(i)* retrieve the ground-truth 3D deformed shape, *(ii)* recover the right spatial domain of non-zero deforming forces. *(iii)* It also proves that we can rigidly place the deformed shape in the image frame without using *SBC*. Finally, we establishes in Proposition 1 that under some conditions the unique ground-truth solution of (RF) is also the unique ground-truth solution of (IF).

2. Related Works and Contributions

Physics-based SfT without sparse prior. The isometry-based SfT [7, 25, 28] requires that any geodesic distance is preserved by the deformation. This approach has proven its accuracy for paper-like surfaces [9]. Conformal-based SfT imposes a local isotropy constraint on the deformations. It was tested on ball-like shapes [19, 9]. For a detailed study of these two geometric-based SfT we recommend [4]. Elastic-based SfT constrains the shape to undergo linear or non-linear elastic deformations. [21] proposed an non-linear iterative SfT method using linear elasticity. The approach relies on stretching energy minimization under re-projection boundary conditions. This method was then cast as a linear problem [20] which can be solved in one optimization run.[14] used a non-linear iterative method based on non-linear elasticity and orthographic projection. [15] used shape contours as *RBC* to estimate both the deformation and the rigid placement of the shape in the deformed image frame.

A close approach to SfT but conceptually different is NRSfM (Non-Rigid Structure-from-Motion). In this approach a deformable shape is reconstructed from multi-frame 2D-2D correspondences. Most of these methods model the deformations using low-rank shapes [10]. A sequential framework which jointly estimate shape and camera poses from multi-image frames was proposed in [2]. This method relies on the Navier-Stokes fluid-flow model. It makes use of FEM to represent the surface and approximates the deformation forces with Gaussians. Both the shape and the forces are reconstructed using an EKF (Extended Kalman Filter).

Statistical-based SfT with sparse prior. Sparsity is famous in computer vision for solving classification problems [32, 30, 33]. Up to now and to the best of our knowledge it was used only in statical-based SfT. It was mainly attempted for human pose estimation. [26] proposed a sparse representation of shape basis to reconstruct 3D human pose from annotated landmarks in a still image. [12] enforces locality when building the pose dictionary. Recently [34] proposes a convex relaxation of the problem of jointly estimating shape and camera pose.

3. Surface Parameterization with FEM

We use shape functions in a finite elements (FEM) framework [8] to represent both the surface and the deformation. This is particularly adapted to elastic SfT and allows to cast it as a linear problem. The finite discrete set of point correspondences has a natural boundary condition through the *RBC*. Any other point of the surface is free from this boundary condition and is subject to the linear elastic prior. Thus let $\mathcal{N}$ be this discrete set of point correspondences between the template and the deformed surface and $n = |\mathcal{N}|$ be its cardinal. In FEM vocabulary, these points are knowns as the nodes of the elements which are used to mesh the surface. We denote $\mathcal{M}$ the set of elements which compose the surface and $m = |\mathcal{M}|$ the total number of elements.

The template surface is denoted $\mathcal{S}_0 \subset \mathbf{R}^{3n}$. A subset of n points $\mathcal{P} \triangleq \left\{ \underline{\mathbf{p}}_i \in \mathcal{S}_0 \right\}_{i=1}^{n}$ are taken to be nodes of the finite element meshing. The template global node vector $\mathbf{p} \in \mathbf{R}^{3n}$ is obtained by stacking column-wise the coordinates of the node points. These coordinates are expressed in the frame of the deformed image. Any point $\underline{\mathbf{p}} \in \mathcal{S}_0$ of the surface is expressed with respect to the n nodes as:

$$\underline{\mathbf{p}}(u,v) = \sum_{i=1}^{n} h_i(u,v)\, \underline{\mathbf{p}}_i,\ i \in [3n], \tag{1}$$

where $[3n] \triangleq \{1, \ldots, 3n\}$ and $(u,v) \in \mathbf{R}^2$ is a global parameterization of the surface. $\{h_i(u,v)\}_{i \in [3n]}$, are real valued differentiable functions called shape functions [8]. The support of h_i is the union of elements that contains node i. The shape functions must sum to one for all u, v. The deformed surface is denoted $\mathcal{S} \subset \mathbf{R}^3$. Defining $\mathcal{S}$ is equivalent to determining the vector field $(\delta : \mathcal{S}_0 \rightarrow \mathbf{R}^{3n} : \underline{\mathbf{p}} \mapsto \underline{\mathbf{x}})$ such that $\mathcal{S} = \left\{ \underline{\mathbf{p}} + \delta(\underline{\mathbf{p}}) = \underline{\mathbf{p}} + \underline{\mathbf{x}}, \underline{\mathbf{p}} \in \mathcal{S}_0,\ \underline{\mathbf{x}} \in \mathbf{R}^{3n} \right\}$. Here $\underline{\mathbf{x}}$ denotes the deformation vector associated to the point $\underline{\mathbf{p}} \in \mathcal{S}_0$. Taking into account the set $\mathcal{P}$ of n nodes, The associated set of deformation vector is defined as $\mathcal{D} \triangleq \left\{ \underline{\mathbf{x}}_i \in \mathbf{R}^{3n} \right\}_{i=1}^{n}$. With isoparameteric FEMs, a deformation $\underline{\mathbf{x}} \in \mathbf{R}^3$ of a given point $\underline{\mathbf{p}} \in \mathcal{S}_0$ is expressed similarly as in (1) with respect to the elements of the set deformation vector $\mathcal{D}$ and the same set shape functions

$$\underline{\mathbf{x}}(u,v) = \sum_{i=1}^{n} h_i(u,v)\, \underline{\mathbf{x}}_i,\ i \in [3n]. \tag{2}$$

The global deformation vector of the nodes $\mathbf{x} \in \mathbf{R}^{3n}$ is obtained by stacking column-wise the coordinates of the deformation vector of the node points. The global node vector of the deformed shape can be represented as $\mathbf{p}+\mathbf{x}$ in the deformed image frame. The reprojection of these points onto the image plane must fit the corresponding point of the template. The obtained linear constraint is called Reprojection Boundary Constraint (*RBC*) and is developed in the following paragraph.

4. Physics and Prior Constraints

4.1. The Reprojection Boundary Constraint

Lets take a single node $\underline{\mathbf{p}}_i \in \mathcal{P}$ from the template surface with coordinates $\underline{\mathbf{p}}_i = \begin{pmatrix} x_i^0 & y_i^0 & z_i^0 \end{pmatrix}^\star$ (the star symbol denotes here the vector and matrix transpose). The coordinates of the corresponding deformation vector are denoted $\underline{\mathbf{x}}_i = \begin{pmatrix} x_i & y_i & z_i \end{pmatrix}^\star$. The point correspondence between template and deformed surface is known and given by the value of the 3D-2D warp at this point $\eta : \mathcal{S}_0 \to \mathbf{\Pi}\mathcal{S} : \underline{\mathbf{p}}_i \mapsto \eta(\underline{\mathbf{p}}_i) = \begin{pmatrix} \eta_i^u & \eta_i^v \end{pmatrix}^\star$. Where $\mathbf{\Pi}\mathcal{S} \subset \mathbf{R}^2$ is the projected domain of the deformed surface. We use perspective projection and assume that the effect of the camera intrinsics are removed on the projected coordinates. The resulted equation can be written as

$$\mathbf{\Pi}_i \, \underline{\mathbf{x}}_i = \underline{\mathbf{y}}_i. \tag{3}$$

Where,

$$\mathbf{\Pi}_i = \begin{pmatrix} 1 & 0 & -\eta_i^u \\ 0 & 1 & -\eta_i^v \end{pmatrix} \text{ and } \underline{\mathbf{y}}_i = -\mathbf{\Pi}_i \underline{\mathbf{p}}_i. \tag{4}$$

Taking into account the n nodes as point correspondences, we obtain an n-block diagonal matrix equation with respect to the global deformation vector $\mathbf{x} \in \mathbf{R}^{3n}$

$$\mathbf{\Pi} \, \mathbf{x} = \mathbf{y}. \tag{5}$$

The global matrix $\mathbf{\Pi} \in \mathbf{R}^{2n \times 3n}$ and global vector $\mathbf{y} \in \mathbf{R}^{2n}$ are written as:

$$\mathbf{\Pi} = \begin{pmatrix} \mathbf{\Pi}_1 & & \mathbf{0} \\ & \ddots & \\ \mathbf{0} & & \mathbf{\Pi}_n \end{pmatrix} \text{ and } \mathbf{y} = \begin{pmatrix} \underline{\mathbf{y}}_1 \\ \vdots \\ \underline{\mathbf{y}}_n \end{pmatrix}. \tag{6}$$

4.2. The Physics of Deformation

A deformation vector $\underline{\mathbf{x}} \in \mathbf{R}^3$ is due to a deforming force vector $\underline{\mathbf{f}} \in \mathbf{R}^3$. Taking into account the set $\mathcal{D}$ of n deformation vector of the nodes, The associated set of deforming force vector is defined as $\mathcal{F} \triangleq \left\{ \underline{\mathbf{f}}_i \in \mathbf{R}^3 \right\}_{i=1}^n$. The global force vector of the nodes $\mathbf{f} \in \mathbf{R}^{3n}$ is obtained by stacking column-wise the coordinates of the deformation vector of the node points. The relation between the global deforming force vector $\mathbf{f}$ and the global deformation vector $\mathbf{x}$ is written as

$$\mathbf{f} = \mathbf{K} \, \mathbf{x}, \tag{7}$$

$\mathbf{K}$ is the stiffness matrix of size $3n \times 3n$, see for instance [20, 2] for the construction of $\mathbf{K}$. This construction can use for instance plate theory [6] if we assume that the addressed surface has locally planar properties (2-manifolds). By construction, matrix $\mathbf{K}$ is symmetric positive semi-definite. We further assume that it satisfies the following two properties

Property 1. *If we assume that we have a regular meshing of the surface [11], then the stiffness matrix $\mathbf{K}$ is well conditioned.*

Property 2. *If we assume that the shape functions satisfy the completeness property [18], then* $\mathrm{rank}(\mathbf{K}) = 3n - 6$. *The null space of dimension* 6 *can be parameterized by a set of three rotations and 3-vector of translation (rigid deformation vector). We denote* $\mathbf{N} \in \mathbf{R}^{3n \times 6}$ *the matrix obtained by concatenating a set of vector basis of this null space*

$$\mathbf{N} = \begin{pmatrix} \mathbf{v}_1 & \dots & \mathbf{v}_6 \end{pmatrix},$$
$$s.t. \ \mathbf{K}\mathbf{v}_i = 0, \ i \in [6], \tag{8}$$
$$\mathbf{v}_1, \dots, \mathbf{v}_6 \ are \ linearly \ independent.$$

The completeness of the shape function ensures that rigid transformations of the template surface $\mathcal{S}_0$ does not involve a deforming force. The only non-zero deforming force is due to non-rigid deformation.

4.3. Support and Sparsity of Deforming Force

Definition 1. *We call the support of $\mathbf{f}$, the location of non-zero elements of its components*

$$\mathcal{Q} \triangleq \{i| \ f_i \neq 0, \ i \in [3n]\}, \tag{9}$$

The size of the support being its cardinal

$$|\mathcal{Q}| \triangleq \|\mathbf{f}\|_0. \tag{10}$$

$\|\cdot\|_0$ is the ℓ_0-norm. f_i is the $i-$th component of $\mathbf{f}$. We denote by $\bar{\mathcal{Q}}$ the complement of $\mathcal{Q}$ in $[3n]$. In the case of sparse deformation, the cardinal $|\mathcal{Q}|$ is expected to be far smaller than $|\bar{\mathcal{Q}}|$.

5. Previous formulation: the ℓ_2-norm Formulation

As was stated in [20] SfT can be formalized as finding $\hat{\mathbf{x}}$ such that

$$\hat{\mathbf{x}} \in \underset{\tilde{\mathbf{x}} \in \mathbf{R}^{3n}}{\arg\min} \frac{1}{2} \|\mathbf{K} \, \tilde{\mathbf{x}}\|_2^2 \text{ s.t. } \begin{cases} \mathbf{\Pi} \, \tilde{\mathbf{x}} = \mathbf{y} & RBC, \\ \mathbf{S} \, \tilde{\mathbf{x}} = \mathbf{0} & SBC. \end{cases} \tag{11}$$

$\mathbf{S}$ is an $l \times 3n$ sparse matrix. It adds l equality constraints on the depth besides the corresponding $2l$ equations of *RBC*.

It was proven in [20] that to have a unique solution with this formulation, it is necessary and sufficient to have l equations of solid boundary constraints such that the matrix $\mathbf{K}$ becomes full rank when updated with the following equations

$$\begin{aligned} \mathbf{K}(3i, 3j) &= 1, & \text{if } i = j, \\ \mathbf{K}(3i, 3j) &= 0, & \text{otherwise.} \end{aligned} \tag{12}$$

Here, i runs over the l solid boundary points and j runs over the $3n$ columns.

6. Formulation of the SLE-SfT

6.1. Removing the SBC

The necessary usage of *SBC* is of limited interest in real world application. They are indeed difficult to set in real context unless setting them by hand or by some artificial markers. In this work, we remove *SBC* from the formulation (11) and we prove, up to a certain level of sparsity, that it is possible to recover the ground-truth solution with the correct support. Without *SBC*, $\mathbf{K}$ is of rank $n-6$ and if $\mathbf{x}$ is a non-rigid deformation, then there is an infinite number of rigid transformations of the surface that obeys the same deforming force $\mathbf{f}$, *i.e.*,

$$\mathbf{f} = \mathbf{K}(\mathbf{x} + \mathbf{N}\mathbf{w}), \text{ for all } \mathbf{w} \in \mathbf{R}^6. \tag{13}$$

Taking into account this equation with the sparsity prior on the deforming force gives rise to the following formulation.

6.2. Ideal Formulation of the SLE-SfT (IF)

Let us denote by $\mathbf{K}^+$ the Moore-Penrose pseudo-inverse matrix of $\mathbf{K}$ [5]. If we remove *SBC* and take into account the sparsity of $\mathbf{f}$, then we obtain the following formulation labelled (IF)

$$\begin{cases} \hat{\mathbf{x}} = \mathbf{K}^+\hat{\mathbf{f}} - \mathbf{N}\hat{\mathbf{w}}, \\ \text{where,} \\ \left(\hat{\mathbf{f}}, \hat{\mathbf{w}}\right) \in \underset{\tilde{\mathbf{f}}, \tilde{\mathbf{w}}}{\arg\min} \left\|\tilde{\mathbf{f}}\right\|_0 \text{ s.t. } \begin{cases} \mathbf{\Pi}\left(\mathbf{K}^+\tilde{\mathbf{f}} + \mathbf{N}\tilde{\mathbf{w}}\right) = \mathbf{y}, \\ \tilde{\mathbf{f}} \in \text{span}(\mathbf{K}). \end{cases} \end{cases}$$
(IF)

By Property 1, we can assume that the computation of $\mathbf{K}^+$ is numerically stable. The additional condition $\tilde{\mathbf{f}} \in \text{span}(\mathbf{K})$ is used here to ensure that (13) is verified. Although this formulation is ideal to exploit the sparsity of $\mathbf{f}$, it has two characteristics that can be simplified: *(i)* the ℓ_0-norm is NP-hard [13]. *(ii)* If the proposed formulation retrieve the unique ground-truth $\mathbf{f}$, then it must satisfy $\tilde{\mathbf{f}} \in \text{span}(\mathbf{K})$. Thus we can simplify the formulation (IF) by: *(i)* using a relaxed formulation with ℓ_1-norm instead of ℓ_0-norm and *(ii)* removing the condition $\tilde{\mathbf{f}} \in \text{span}(\mathbf{K})$. This final formulation can be stated in the following paragraph. The solution of the final problem is relevant if and only if it is the ground-truth solution and thus equal to the solution of the ideal formulation. This solution equality and the condition under which it is true are established in Proposition 1 in Section 7.2.

6.2.1 Relaxed Formulation of the SLE-SfT (RF)

The relaxed formulation without the condition on $\mathbf{f}$ being in span($\mathbf{K}$) is denoted (RF) and is given by

$$\begin{cases} \hat{\mathbf{x}} = \mathbf{K}^+\hat{\mathbf{f}} - \mathbf{N}\hat{\mathbf{w}}, \\ \text{where,} \\ \left(\hat{\mathbf{f}}, \hat{\mathbf{w}}\right) \in \underset{\tilde{\mathbf{f}}, \tilde{\mathbf{w}}}{\arg\min} \left\|\tilde{\mathbf{f}}\right\|_1 \text{ s.t. } \mathbf{\Pi}\left(\mathbf{K}^+\tilde{\mathbf{f}} + \mathbf{N}\tilde{\mathbf{w}}\right) = \mathbf{y}. \end{cases}$$
(RF)

The global scheme of this minimization problem corresponds to an ℓ_1 linear convex problem with linear constraint. If this problem has a unique solution if the feasible set is non-empty, it is not always the case that this solution corresponds to the ground-truth solution. Deriving conditions under which this solution is the ground-truth solution allows us to prove that the solution of (RF) is the same as the one of (IF). Though it has been widely studied in the theory of compressive sensing [13], it was never been proposed in the field of SfT for sparse deforming force. The following theoretical results are derived from this theory. In particular, the proofs of Theorems 1 and 2 below are derived from those in [13] to the specific SLE-SfT problem.

7. Exact Recovery Condition for (RF)

In this section we want to establish the exact recovery condition for (RF) where the unique estimated solution $\hat{\mathbf{x}}$ via this formulation is equal to the ground-truth deformation $\mathbf{x}$. For this purpose, we first give an extension of the definition of the Null Space Property. This property is famous in compressive sensing [13] and allows us to provide necesseray and sufficient conditions for ℓ_1-norm relaxed problems.

7.1. The Projective Elastic Space Property (PESP)

Let us denote $\mathbf{f}_{\mathcal{Q}} \in \mathbb{R}^{|\mathcal{Q}|}$ and $\mathbf{f}_{\bar{\mathcal{Q}}} \in \mathbb{R}^{|\bar{\mathcal{Q}}|}$ as the restrictions of $\mathbf{f}$ to the indices in $\mathcal{Q}$ and $\bar{\mathcal{Q}}$ respectively.

Definition 2. *We say that the couple* $(\mathbf{\Pi}, \mathbf{K})$ *satisfies the Projective Elastic Space Property (PESP) relative to* $\mathcal{Q} \subset [3n]$ *if for every* $\mathbf{f} \in \mathbb{R}^{3n}\backslash\{0\}$ *such that* $\mathbf{\Pi}\mathbf{K}^+\mathbf{f} \in$ span($\mathbf{\Pi}\mathbf{N}$), *we have*

$$\|\mathbf{f}_{\mathcal{Q}}\|_1 < \|\mathbf{f}_{\bar{\mathcal{Q}}}\|_1. \tag{14}$$

This definition is an extension of the more generic modified Null Space Property [3, 13]. This definition is concerned with all the non-zero forces $\mathbf{f}$ such that the perspective projection of a non-rigid deformation can be explained by a perspective projection of a rigid transformation. If the couple $(\mathbf{\Pi}, \mathbf{K})$ satisfies the PESP for a given $\mathcal{Q} \subset [3n]$, then the restriction of such force to $\mathcal{Q}$ is strictly dominated by the restriction of this force to $\bar{\mathcal{Q}}$ in the sense of the ℓ_1-norm. We say that it satisfies the PESP of order s if it satisfies the PESP relative to any support $\mathcal{Q} \subset [3n]$ with card($\mathcal{Q}$) $\leq s$.

Theorem 1. *Every couple* $(\mathbf{f}, \mathbf{w}) \in \mathbb{R}^{3n} \times \mathbb{R}^6$, *where the force vector* $\mathbf{f}$ *is supported on a set* $\mathcal{Q}$, *is the unique solution*

of (RF) *with the observed image* $\mathbf{y} = \mathbf{\Pi}(\mathbf{K}^+\mathbf{f} + \mathbf{N}\mathbf{w})$ *if and only if the couple* $(\mathbf{\Pi}, \mathbf{K})$ *satisfies the PESP relative to* $\mathcal{Q}$. *The unique reconstructed deformation is thus given by* $\mathbf{x} = \mathbf{K}^+\mathbf{f} - \mathbf{N}\mathbf{w}$.

The strength of this theorem is to state that satisfying the PESP relative to a support $\mathcal{Q}$ is necessary and sufficient to retrieve the ground-truth solution $\mathbf{x}$ and $(\mathbf{f}, \mathbf{w})$ via (RF). To prove this theorem, we first need the following lemma

Lemma 1. *For any* $n > 3$, *a given* $\mathbf{\Pi}$ *and* $\mathbf{N}$ *as defined respectively in* (6) *and* (8), *we have*

$$\ker(\mathbf{\Pi}\mathbf{N}) = \{0\}. \tag{15}$$

Proof. Let us consider $\mathbf{p} \in \mathbb{R}^{3n}$ as the node points of the template surface $\mathcal{S}_0$. If we consider that there exists $\mathbf{w} \in \ker(\mathbf{\Pi}\mathbf{N})$ such that $\mathbf{w} \neq 0$. Then this is equivalent to saying that there exists a rigid displacement $\mathbf{N}\mathbf{w} \neq 0$ of the template nodes $\mathbf{p}$ that does not change their initial projection

$$\mathbf{\Pi}(\mathbf{N}\mathbf{w} + \mathbf{p}) = \mathbf{\Pi}\mathbf{p}. \tag{16}$$

Which means that $\mathbf{\Pi}\mathbf{N}$ is injective. As a matter of fact, a rigid positioning of a set of n points to fit a given perspective projection is nothing but a PnP problem [24]. It has been established [16] that for $n > 3$, there is no rigid transformation of $\mathbf{p}$ that can give similar perspective projection as stated in (16) which is a contradiction with the hypothesis $\mathbf{w} \neq 0$. $\quad\square$

In this paper, we study our new formulation for generic cases where $n > 3$. The case $n \leq 3$ is a very specific study that requires more care. We let this case for later development as potential futur work. The proof of Theorem 1 is thus given as follows.

Proof. Let us first prove the necessity of PESP. Given a known support set $\mathcal{Q}$, let assume that every couple $(\mathbf{f}, \mathbf{w}) \in \mathbb{R}^{3n} \times \mathbb{R}^6$, where $\mathbf{f}$ is supported on a set $\mathcal{Q}$, is the unique minimizer of $\left\|\tilde{\mathbf{f}}\right\|_1$ subject to $\mathbf{\Pi}\left(\mathbf{K}^+\tilde{\mathbf{f}} + \mathbf{N}\tilde{\mathbf{w}}\right) = \mathbf{\Pi}(\mathbf{K}^+\mathbf{f} + \mathbf{N}\mathbf{w})$. Particularly, if $\mathbf{f} \in \mathbb{R}^{3n}$ is any vector (not necessarily supported on $\mathcal{Q}$) such that $\mathbf{\Pi}\mathbf{K}^+\mathbf{f} \in \mathrm{span}(\mathbf{\Pi}\mathbf{N})$, then by the assumption we have that $(\mathbf{f}_\mathcal{Q}, \mathbf{w})$ is the unique minimizer of $\left\|\tilde{\mathbf{f}}\right\|_1$ subject to $\mathbf{\Pi}\left(\mathbf{K}^+\tilde{\mathbf{f}} + \mathbf{N}\tilde{\mathbf{w}}\right) = \mathbf{\Pi}(\mathbf{K}^+\mathbf{f}_\mathcal{Q} + \mathbf{N}\mathbf{w})$. Since $\mathbf{\Pi}\mathbf{K}^+\mathbf{f} \in \mathrm{span}(\mathbf{\Pi}\mathbf{N})$, there exists a unique $\mathbf{w}' \in \mathbb{R}^6$ (thanks to Lemma 1) such that $\mathbf{\Pi}\mathbf{K}^+\mathbf{f} = \mathbf{\Pi}\mathbf{N}\mathbf{w}'$. If we choose $\tilde{\mathbf{w}} = \mathbf{w}' + \mathbf{w}$ and write $\mathbf{f} = \mathbf{f}_\mathcal{Q} + \mathbf{f}_{\bar{\mathcal{Q}}}$ then we find that $(\mathbf{f}_{\bar{\mathcal{Q}}}, \tilde{\mathbf{w}})$ is a feasible solution. Since by assumption $(\mathbf{f}_\mathcal{Q}, \mathbf{w})$ is the unique minimizer, we must have $\|\mathbf{f}_\mathcal{Q}\|_1 < \|\mathbf{f}_{\bar{\mathcal{Q}}}\|_1$ which establishes the PESP relative to $\mathcal{Q}$ for the couple $(\mathbf{\Pi}, \mathbf{K})$.

Let us now prove the sufficiency of PESP. Let assume that the couple $(\mathbf{\Pi}, \mathbf{K})$ satisfies the PESP relative to a given set $\mathcal{Q} \subset [3n]$. For a given couple $(\mathbf{f}, \mathbf{w}) \in \mathbb{R}^{3n} \times \mathbb{R}^6$, where $\mathbf{f}$ is supported on $\mathcal{Q}$ and any other feasible couple $\left(\tilde{\mathbf{f}}, \tilde{\mathbf{w}}\right) \in$

$\mathbb{R}^{3n} \times \mathbb{R}^6$ satisfying $\mathbf{\Pi}\left(\mathbf{K}^+\tilde{\mathbf{f}} + \mathbf{N}\tilde{\mathbf{w}}\right) = \mathbf{\Pi}(\mathbf{K}^+\mathbf{f} + \mathbf{N}\mathbf{w})$, we can easily check that the vector $\mathbf{v} \triangleq \mathbf{f} - \tilde{\mathbf{f}}$ is such that $\mathbf{\Pi}\mathbf{K}^+\mathbf{v} \in \mathrm{span}(\mathbf{\Pi}\mathbf{N})$. Thus we can use the PESP with $\mathbf{v}$ to prove that

$$\begin{aligned}
\|\mathbf{f}\|_1 &= \left\|\mathbf{f} - \tilde{\mathbf{f}}_\mathcal{Q} + \tilde{\mathbf{f}}_\mathcal{Q}\right\|, \\
&\leq \left\|\mathbf{f} - \tilde{\mathbf{f}}_\mathcal{Q}\right\|_1 + \left\|\tilde{\mathbf{f}}_\mathcal{Q}\right\|_1, \text{ by triangular inequality} \\
&= \|\mathbf{v}_\mathcal{Q}\|_1 + \left\|\tilde{\mathbf{f}}_\mathcal{Q}\right\|_1, \text{ by definition of } \mathbf{v} \\
&< \|\mathbf{v}_{\bar{\mathcal{Q}}}\|_1 + \left\|\tilde{\mathbf{f}}_\mathcal{Q}\right\|_1, \text{ by PESP on } \mathbf{v} \\
&= \left\|\tilde{\mathbf{f}}_{\bar{\mathcal{Q}}}\right\|_1 + \left\|\tilde{\mathbf{f}}_\mathcal{Q}\right\|_1, \text{ since } \mathbf{f} = \mathbf{f}_\mathcal{Q}, \mathbf{f}_{\bar{\mathcal{Q}}} = 0 \\
&= \left\|\tilde{\mathbf{f}}\right\|_1. \tag{17}
\end{aligned}$$

This concludes that $\mathbf{f}$ is the unique minimizer of (RF). If $\tilde{\mathbf{w}} \in \mathbb{R}^6$ is a feasible solution then $\mathbf{\Pi}\mathbf{N}\tilde{\mathbf{w}} = \mathbf{y} - \mathbf{\Pi}\mathbf{K}^+\mathbf{f} = \mathbf{\Pi}\mathbf{N}\mathbf{w}$. By Lemma 1, $\mathbf{\Pi}\mathbf{N}$ is injective and then $\tilde{\mathbf{w}} = \mathbf{w}$. $\quad\square$

Theorem 2. *Every couple* $(\mathbf{f}, \mathbf{w}) \in \mathbb{R}^{3n} \times \mathbb{R}^6$, *where* $\mathbf{f}$ *is an* s-*sparse force vector, is the unique solution of* (RF) *with the observed image* $\mathbf{y} = \mathbf{\Pi}(\mathbf{K}^+\mathbf{f} + \mathbf{N}\mathbf{w})$ *if and only if the couple* $(\mathbf{\Pi}, \mathbf{K})$ *satisfies the PESP of order* s. *The unique reconstructed deformation is thus given by* $\mathbf{x} = \mathbf{K}^+\mathbf{f} - \mathbf{N}\mathbf{w}$.

Proof. If $(\mathbf{\Pi}, \mathbf{K})$ satisfies the PESP of order s then by definition it satisfies the PESP relative to any support $\mathcal{Q} \subset [3n]$ with $\mathrm{card}(\mathcal{Q}) \leq s$. Hence for every such support $\mathcal{Q}$ and by Theorem 1 every couple $(\mathbf{f}, \mathbf{w}) \in \mathbb{R}^{3n} \times \mathbb{R}^6$, where $\mathbf{f}$ is supported on $\mathcal{Q}$, is the unique solution of (RF). $\quad\square$

7.2. Exact Recovery for (IF)

Proposition 1. *Under the condition of Theorem 2 every recovered ground-truth solution via problem* (RF) *is also the unique ground-truth solution of problem* (IF).

Proof. Under the condition of Theorem 2, the recovered solution corresponds to the ground-truth solution $(\mathbf{f}, \mathbf{w})$, where $\mathbf{f}$ is s-sparse. By hypothesis, this force $\mathbf{f} \in \mathbb{R}^{3n}$ causes the deformation and satisfies the model $\mathbf{f} = \mathbf{K}\mathbf{x}$ which stands for $\mathbf{f} \in \mathrm{span}(\mathbf{K})$. Moreover, let $(\mathbf{z}, \mathbf{c})$ be the minimizer of (IF) with $\mathbf{y} = \mathbf{\Pi}\left(\mathbf{K}^+\tilde{\mathbf{f}} + \mathbf{N}\tilde{\mathbf{w}}\right)$ then $\|\mathbf{z}\|_0 \leq \|\mathbf{f}\|_0$ so that $\mathbf{z}$ is also s-sparse. Since every s-sparse vector is the unique solution of (RF) with the same $\mathbf{y} = \mathbf{\Pi}\left(\mathbf{K}^+\tilde{\mathbf{f}} + \mathbf{N}\tilde{\mathbf{w}}\right)$, it follows that $\mathbf{f} = \mathbf{z}$. We have $\tilde{\mathbf{w}} = \mathbf{c}$ because of Lemma 1. $\quad\square$

8. Implementation and Compared Methods

The method implementation and evaluation used MATLAB R2014A running upon a MAC PRO (OS X 10.11.4) with INTEL CORE I5 running at 2×2.66 GHz with 8 GB DDR3 memory. The resolution of the constrained ℓ_1 minimization part of (RF) was implemented using ADMM

algorithm[31]. The Alternating Direction Method of Multipliers (ADMM) is an algorithm that solves linear convex optimization problems by breaking them into smaller pieces, each of which are then easier to handle. We used triangular elements and polynomial shape functions to describe the finite element meshing of the surface [8]. We used a plate model to describe the mechanics of the deformable surface [6]. This model is valid as soon as the thickness of the surface remains negligible when compared to the maximum side length of a single triangular element. For each material used in the experiments, we used its mechanical parameters represented by the Poisson's ratio ν and Young modulus E. These parameters with the shape functions are used to compute the stiffness matrix $\mathbf{K}$ [20, 2].

To illustrate quantitatively and qualitatively the benefits of the proposed SLE-SfT, we compared five methods: *(1)* **SLE**, the proposed method through the resolution of (RF). *(2)* **LM** [20], a linear iterative method that minimizes the ℓ_2-norm of the force. *(3)* **NLM** [21], a non-linear iterative method that minimizes the elastic energy of deformation. *(4)* **KFM** [2], a sequential method that uses mechanical priors embedded in a Kalman Filtering process. *(5)* **AG** [4], an analytic method that uses conformal prior as geometric constraints. We do not compare to methods that use isometric prior since the deformations that we study are non-isometric.

To compare the proposed methods to those that use *SBC*, namely **LM** and **NLM**, we mimicked their approach in using *SBC* to position the template in the deformed image. We thus set $\mathbf{K}$ to be full rank as shown in (12). The pseudo-inverse is replaced by the inverse matrix and $\mathbf{N}$ is set to zero. For fair comparison, we did not compare **SLE** to **LM** and **NLM** in the case of datasets that did not make usage of *SBC*.

9. Experimental Evaluation

9.1. Synthetic Data

In order to fit the linear elastic model, each deformed element triangle has an increasing area rate of at most 25% than the template element triangle (triangle at rest) [20]. We used 3D STUDIO MAX [22] to simulate plausible deformed surfaces. We used a balloon-like synthetic material with Poisson's ratio $\nu = 0.50$ and Young's modulus $E = 10^3$ Pa[1]. The template surface was planar and of size 90×90 mm^2. We sampled it in a regular triangular grid of $n = 100$ nodes and 162 special right triangle faces. The perpendicular sides are of length 10 mm each and the hypotenuse being $10\sqrt{2}$ mm. We choosed a thickness of $h = 0.75$ mm such that it fits the local plate mechanical model []. The generated deformations were completely free from such constraint. The sparse deforming forces are applied at some nodes of the mesh. Their magnitude and orientation are randomly generated. The magnitude is generated with a centered Gaussian distribution of standard deviation of 5 Newton. The orientations follows a uniform distribution. The non-rigidly deformed surface was also moved with rigid transformations. They were randomly generated with uniform distributions for translations and rotations. The nodes of the simulated deformed surfaces are projected with a perspective projection. The center of projection was in average at a distance of 300 mm from the closest point on the surface. We generated two sets of data: one set with *SBC* at the border of the square and a second set without *SBC* at the boundary. For each of them, we ran two sets of test; *(i)* varying image noise: centred Gaussian noise $\mathcal{N}_{\mathcal{Q}}$ with varying standard deviation $\sigma = [0 : 1 : 4]^2$ pixels was added to the image points. *(ii)* varying size of support s: we used uniformly random generated supports with varying sizes $|\mathcal{Q}| = [1 : 1 : 3 \ \ 5 : 5 : 200]$. It makes 430 different experimental setup that we ran with 500 samples to obtain a representative result. We measure the reconstruction accuracy with two criteria: *(i)* The ratio of the size of exactly recovered locations of zeros of the force to the total size of the force vector. *(ii)* The 3D residual error in mm between the generated deformed 3D points and the reconstructed 3D points. **SLE** methods shows substantial improvement especially when the support size s is less than 30% of the total size of the force vector, *i.e.*, $s \leq 0.3(3n)$. figure 1 summarizes the obtained results with the synthetic data. figure 1-(a) reveals the rate of recovery of the locations of zeros in the force vector $\mathbf{f}$. It shows that **SLE** recovers exact location when sparsity goes to 45% of the total size of the vector (135 among 300 components). This rate naturally decreases when the noise increases. However, **SLE** presents more stable recovery than the compared methods. The other methods are more sensitive to noise and generally fail to recover these locations in presence of noise. **KFM** uses the force as noise embedded in an Extended Kalman Filter framework. For this reason, the force is not used in the field of its physical meaning and then the method cannot provide the correct support of $\mathbf{f}$. **LM** is an ℓ_2-norm formulation and in presence of noise it tends to find the best tradeoff among data in the sense of least squares. Thus polluting the estimated $\mathbf{f}$ with false negative non-zero locations in the the complement of the support $\bar{\mathcal{Q}}$. In this figure we do not compare **AG** and **NLM** since they dont make usage of any force modelling. figure 1-(b) shows quantitative comparison of accuracy of the 3D reconstruction for each method. Method **SLE** demonstrates for this data accuracy in both mean and std 3D errors. This observation is qualitatively confirmed in figure 1-(c).

9.2. Real Data

We used four sets of data with ground-truth that was obtained with stereo calibrated cameras. The two cameras have a resolution of 1920×1080 pixels. A set of 15 deformed shapes was used for each dataset. The four datasets were subdivided into two classes. The first class was experimented with *SBC* and contained: *(1)* **cup-lid** dataset composed of deformed lid made of silicone rubber material ($\nu = 0.27$, $E = 10^9$ Pa). The boundary of the lid was fixed to the boundary of the cup, see figure 2-(a). The thickness of the material is set to $h = 2$ mm and its bounding box

---
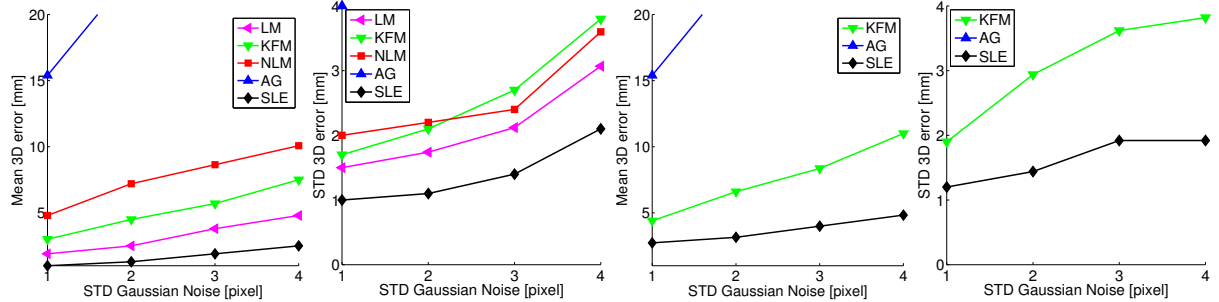
[1]Pa stands for Pascals to measure force per unit area.

[2]As in MATLAB notation: [init:step:final] values.
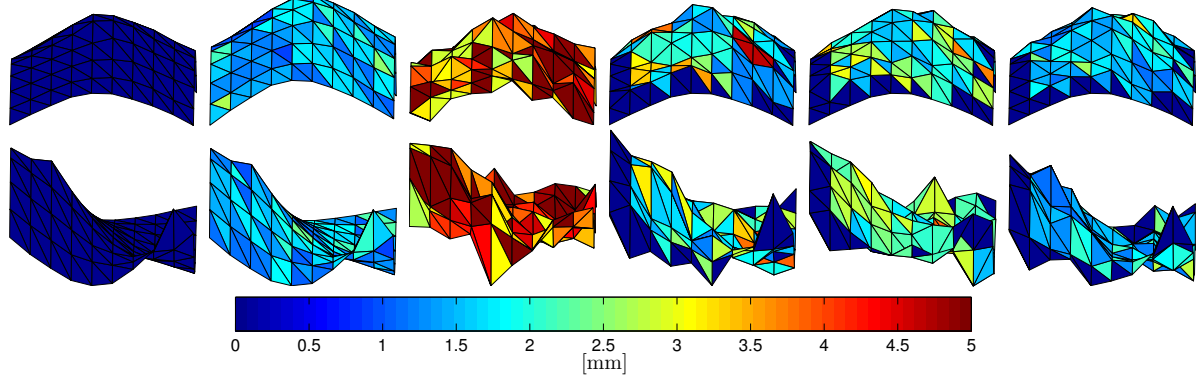
(a) Ratio of correctly recovered locations of zeros in force vector to the total size of this vector.
From left to right: **SLE** and **KFM** without *SBC*. Then **SLE**, **LM** and **KFM** with *SBC*.

(b) Average mean and std 3D error of reconstruction.
Left pair of figures are related to experiment with *SBC*. Right pair of figures are related to those without *SBC*.

(c) SfT reconstructions with errors displayed as heatmaps ($\sigma = 1$). From left to right: ground-truth, **SLE**, **AG**, **KFM**, **NLM**, **LM**.
First row with *SBC*. Second row without *SBC*.

Figure 1. Results on synthetic data. Results of methods with large errors are not shown to fit the average error scale.

size is $50 \times 50 \times 20$ mm^3. *(2)* **strip** dataset composed of deformed band made of polyester material ($\nu = 0.3$, $E = 10^5$ Pa). The two side widths of the strip were fixed to a circular wood, see figure 2-(b). The thickness of the material is set to $h = 1$ mm and its bounding box size is 25×100 mm^2. The second class was experimented without *SBC* and contained: *(3)* **clothes** dataset composed of deformed clothes made of spandex material ($\nu = 0.5$, $E = 10^4$ Pa). The boundary of the clothes were barely maintained by hand to obtain elastic deformation, see figure 2-(c). The thickness of the material is set to $h = 1$ mm and its bounding box size is 200×200 mm^2. *(4)* **balloon** dataset composed of deformed inflated balloon made of rubber material ($\nu = 0.5$, $E = 10^3$ Pa), see figure 2-(d). The thickness of the material is set to $h = 0.5$

mm and its bounding box size is $150 \times 100 \times 20$ mm^3. Feature points are obtained semi-automatically with SIFT [17]. These feature points represents the nodes of the mesh. For the **cup-lid** pattern, we used a total of 500 feature points among which 50 fixed boundary points were used as *SBC* . For the **strip** pattern, we used a total of 350 feature points among which 30 fixed boundary points were used as *SBC* . We used 420 feature points for the **clothes** pattern and 600 feature points for the **balloon** pattern. The ability of recovering the correct support of the deforming force was similar to the results obtained for synthetic data with 10% of the support size and 2 pixels of std Gaussian noise in image features. The mean 3D error was measured at about 1.2 mm for **SLE**, 2.5 mm for **KFM** method, 2.0 mm for **LM**, 3.2 mm

(a.1) **KFM** (a.4) **SLE**

(a.2) **NLM** (a.5) Grd truth

(a.3) **AG** (a.6) **LM**

(a) **Cup-lid** dataset

(b.1) **KFM** (b.4) **SLE**

(b.2) **NLM** (b.5) Grd truth

(b.3) **AG** (b.6) **LM**

(b) **Strip** dataset

(c.1) **KFM** (c.3) **SLE**

(c.2) **AG** (c.4) Grd truth

(c) **Clothes** dataset

(d.1) **KFM** (d.4) **SLE**

(d.3) **AG** (d.5) Grd truth

(d) **Balloon** dataset
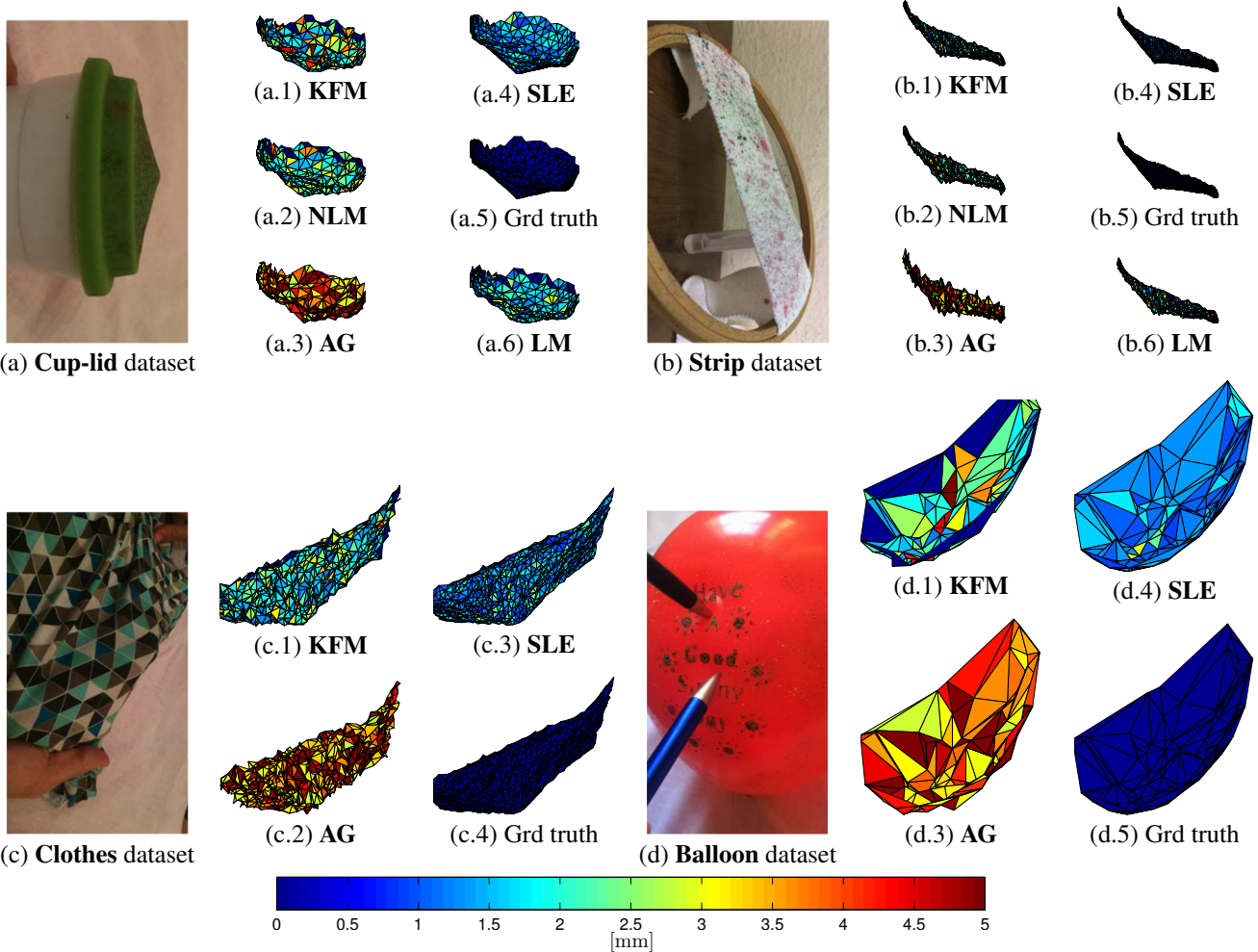
Figure 2. . Results with real data. The reconstruction of the deformation of the balloon are returned up side down to appreciate the creases.

Method	SLE	KFM	LM	NLM	AG
silicone-lid	1.2[1.7]	2.0[3.5]	1.9[2.7]	3.1[2.1]	2.8[3.1]
strip	1.5[2.0]	2.1[2.5]	2.0[2.6]	3.3[2.4]	2.9[2.1]
clothes	1.6[2.1]	2.9[3.5]	-	-	2.8[2.2]
balloon	1.6[1.9]	3.1[3.9]	-	-	3.1[2.6]

Table 1. Reconstruction errors for the real datasets (mean[std] in mm).

for **NLM** and 2.9 mm for **AG**. **SLE** has a remarquable stability through the tight std in the reconstruction error. Table 1 summarizes the statistics of the errors in terms of mean and std of 3D reconstructed points.

10. Conclusion

In this paper we formalized a new class of SfT, namely SLE-SfT, that can handle spatially sparse deforming forces. We used both an ideal ℓ_0-norm formulation and a relaxed ℓ_1-norm formulation. We introduced the PESP (Projec-

tive Elastic Space Property) that allowed us to characterize the exact recovery of both the support of the deforming force and the ground-truth deformed shape. We also proved that if PESP is verified then the solution of the relaxed formulation is the solution of the ideal formulation. We provided experimental results on both synthetic and real data. We showed the effectiveness of the proposed method over state-of-the-art methods. It is worth to notice that the ADMM algorithm used to solve the problem in the current setup is relatively slow. For real-time application, it is worth to investigate the way the current solving method could be speeded-up in a futur development work.

References

[1] A. Agudo and F. Moreno-Noguer. Learning Shape, Motion and Elastic Models in Force Space. *ICCV*, 2015. 1

[2] A. Agudo, F. Moreno-Noguer, B. Calvo, and J. M. M. Montiel. Sequential non-rigid structure from motion

using physical priors. *IEEE Transactions on Pattern Analysis and Machine Intelligence*, 38(5), 2016. 1, 2, 3, 6

[3] A. S. Bandeira, K. Scheinberg, and L. N. Vicente. On partial sparse recovery. *arXiv:1304.2809 [cs, math]*, 2013. 4

[4] A. Bartoli, Y. Grard, F. Chadebecq, T. Collins, and D. Pizarro. Shape-from-Template. *IEEE Transactions on Pattern Analysis and Machine Intelligence*, 37(10):2099–2118, 2015. 1, 2, 6

[5] A. Ben-Israel and T. N. E. Greville. *Generalized Inverses: Theory and Applications*. Springer Science & Business Media, 2006. 4

[6] A. P. Boresi, R. J. Schmidt, and O. M. Sidebottom. *Advanced Mechanics of Materials*. Wiler, 1993. 3, 6

[7] F. Brunet, R. Hartley, A. Bartoli, N. Navab, and R. Malgouyres. Monocular template-based reconstruction of smooth and inextensible surfaces. *ACCV*, 2010. 1, 2

[8] J. Chaskalovic. *Finite Elements Methods for Engineering Sciences*. Springer Verlag, 2008. 2, 6

[9] A. Chhatkuli, D. Pizarro, and A. Bartoli. Stable template-based isometric 3D reconstruction in all imaging conditions by linear least-squares. *CVPR*, 2014. 1, 2

[10] Y. Dai, H. Li, and M. He. A Simple Prior-Free Method for Non-rigid Structure-from-Motion Factorization. *Int. J. Comput. Vision*, 107(2):101–122, 2014. 2

[11] Q. Du, D. Wang, and L. Zhu. On Mesh Geometry and Stiffness Matrix Conditioning for General Finite Element Spaces. *SIAM J. Numer. Anal.*, 47(2):1421–1444, 2009. 3

[12] X. Fan, K. Zheng, Y. Zhou, and S. Wang. Pose Locality Constrained Representation for 3d Human Pose Reconstruction. *ECCV*, 2014. 1, 2

[13] S. Foucart and H. Rauhut. *A Mathematical Introduction to Compressive Sensing*. Springer Science & Business Media, 2013. 2, 4

[14] N. Haouchine, J. Dequidt, M.-O. Berger, and S. Cotin. Single view augmentation of 3D elastic objects. *ISMAR*, 2014. 1, 2

[15] N. Haouchine, F. Roy, L. Untereiner, and S. Cotin. Using Contours as boundary conditions for elastic registration during minimally invasive hepatic surgery. *IROS*, 2016. 2

[16] B. Haralick, C.-N. Lee, K. Ottenberg, and M. Naelle. Review and analysis of solutions of the three point perspective pose estimation problem. *IJCV*, 13(3):331–356, 1994. 5

[17] D. G. Lowe. Distinctive image features from scale-invariant keypoints. *International Journal of Computer Vision*, 60(2):91–110, 2004. 7

[18] E. Madenci and I. Guven. *The Finite Element Method and Applications in Engineering Using ANSYS*. Springer US, Boston, MA, 2015. 3

[19] A. Malti, A. Bartoli, and T. Collins. Template-based conformal shape-from-motion from registered laparoscopic images. *MIUA*, 2011. 1, 2

[20] A. Malti, A. Bartoli, and R. Hartley. A linear least-squares solution to elastic shape-from-template. *CVPR*, 2015. 1, 2, 3, 6

[21] A. Malti, R. Hartley, A. Bartoli, and J.-H. Kim. Monocular template-based 3D reconstruction of extensible surfaces with local linear elasticity. *CVPR*, 2013. 1, 2, 6

[22] M. Matossian. *3D Studio MAX 3: Visual QuickStart Guide*. Peachpit Press, 1999. 6

[23] I. Matthews and S. Baker. Active appearance models revisited. *International Journal of Computer Vision*, 60(2):135–164, 2004. 1

[24] F. Moreno-Noguer, V. Lepetit, and P. Fua. Accurate non-iterative o(n) solution to the pnp problem. *ICCV*, 2007. 5

[25] F. Moreno-Noguer and J. Porta. Probabilistic simultaneous pose and non-rigid shape recovery. *CVPR*, 2011. 1, 2

[26] V. Ramakrishna, T. Kanade, and Y. Sheikh. Reconstructing 3D Human Pose from 2D Image Landmarks. *ECCV*, 2012. 1, 2

[27] M. Salzmann and P. Fua. Reconstructing sharply folding surfaces: A convex formulation. *CVPR*, 2009. 1

[28] M. Salzmann and P. Fua. Linear local models for monocular reconstruction of deformable surfaces. *IEEE Transactions on Pattern Analysis and Machine Intelligence*, pages 931–944, 2011. 1, 2

[29] M. Salzmann and R. Urtasun. Beyond feature points: Structured prediction for monocular non-rigid 3D reconstruction. *ECCV*, 2012. 1

[30] A. Wagner, J. Wright, A. Ganesh, Z. Zhou, H. Mobahi, and Y. Ma. Toward a Practical Face Recognition System: Robust Alignment and Illumination by Sparse Representation. *IEEE Transactions on Pattern Analysis and Machine Intelligence*, 34(2):372–386, 2012. 2

[31] Z. Wen, D. Goldfarb, and W. Yin. Alternating direction augmented Lagrangian methods for semidefinite programming. *Mathematical Programming Computation*, 2(3-4):203–230, 2010. 6

[32] J. Wright, A. Y. Yang, A. Ganesh, S. S. Sastry, and Y. Ma. Robust Face Recognition via Sparse Representation. *IEEE Transactions on Pattern Analysis and Machine Intelligence*, 31(2):210–227, 2009. 2

[33] B. Zhang, A. Perina, V. Murino, and A. Del Bue. Sparse Representation Classification With Manifold Constraints Transfer. *CVPR*, 2015. 2

[34] X. Zhou, S. Leonardos, X. Hu, and K. Daniilidis. 3D shape estimation from 2D landmarks: A convex relaxation approach. *CVPR*, 2015. 1, 2